Chapter

Inner Tapered Tree-Shaped Ultra-Wideband Fractal Antenna with Polarization Diversity

Sarthak Singhal and Amit Kumar Singh

Abstract

A coplanar waveguide (CPW)-fed third iteration inner tapered tree-shaped ultra-wideband (UWB) fractal antenna for polarization diversity applications is presented. The antenna comprises of two orthogonal fractal antenna structures to achieve polarization diversity performance across the frequency spectrum of 4.7–19.4 GHz. An isolation of more than 15 dB is accomplished. The designed antenna has a nearly omnidirectional radiation pattern with an average gain of 2.45 dB, very low values of envelope correlation coefficient and capacity loss, nearly constant diversity gain (DG) and mean effective gain (MEG) values. The time domain analysis results illustrated the low dispersion in the radiated pulse. The designed antenna has advantages of wider bandwidth and miniaturized dimensions along with good diversity performance. These advantages make the designed antenna a promising candidate for future wireless communication systems having multipath fading as a major concern.

Keywords: coplanar waveguide feeding, fractal antenna, polarization diversity antenna, ultra-wideband antenna

1. Introduction

In 2002, FCC allocated the unlicensed frequency spectrum from 3.1 to 10.6 GHz for ultra-wideband (UWB) technology [1]. After this allocation, ultra-wideband has received attention from wireless communication experts owing to its advantageous features like wider bandwidth, low cost, low susceptibility to multipath fading, reduced probability of detection and intercept and potentially high data rates. In a highly dense and dynamic environment, the UWB systems suffer from multipath fading due to reflection and diffraction. This multipath fading results into the degradation of signal-to-noise ratio (SNR) and channel capacity.

An effective method to resolve these multipath fading issues is the incorporation of antenna diversity techniques in wireless communication systems. Several types of diversity, such as space/spatial, pattern and polarization diversity, have been already proposed and implemented to receive multiple signals [2–4].

In a diversity scheme, the power or signal-to-noise ratio of the received signal is optimized by the selection or combining of output signals in several ways like selection combining, equal gain combining or maximal ratio combining. The detailed description of diversity combining techniques is available in [5, 6].

1

IntechOpen

For good diversity performance, the received signals should have very low correlation between them [7]. An increase in correlation reduces the combining efficiency. In a spatial diversity scheme, a large separation (compared to wavelength) between the antennas is used to achieve decoupling between signals. This large space requirement limits the use of this diversity method. To overcome this drawback, other techniques such as pattern or polarization diversity [8, 9] are investigated. These alternate techniques involve the use of two or more antenna elements with different radiation patterns [10]. An UWB system with polarization diversity technique has potential applications in advanced instruments used for microwave imaging, radar and high-speed data transfer. Some UWB polarization diversity antennas are already reported in the literature [11–28]. However, the application of those available structures is limited due to their large dimensions, multilayer structure, complex feedline, complex geometries, etc.

Among the various bandwidth enhancement techniques, the use of fractal geometries is proven to be a good method. Fractal antenna structures have a compact size and wideband performance due to properties of self-similarity, space filling and effective energy coupling properties [29].

In this chapter, a compact CPW-fed UWB fractal antenna with polarization diversity performance is presented. The bandwidth of the antenna structure [29] is enhanced by loading the coplanar ground planes with a quarter wavelength long rectangular notches. Two identical copies of this antenna structure are arranged orthogonally to achieve good interport isolation and orthogonal polarization diversity performance without affecting the UWB performance. In the following sections, antenna design description is followed by discussion of frequency domain analysis results, time domain analysis results and diversity performance parameter calculation. Finally, it is concluded with major findings of this chapter.

2. Antenna design

The geometry of the antenna structure is demonstrated in **Figure 1**, and its optimized dimensions are listed in **Table 1**. It is etched on a 1.6 mm thick FR-4
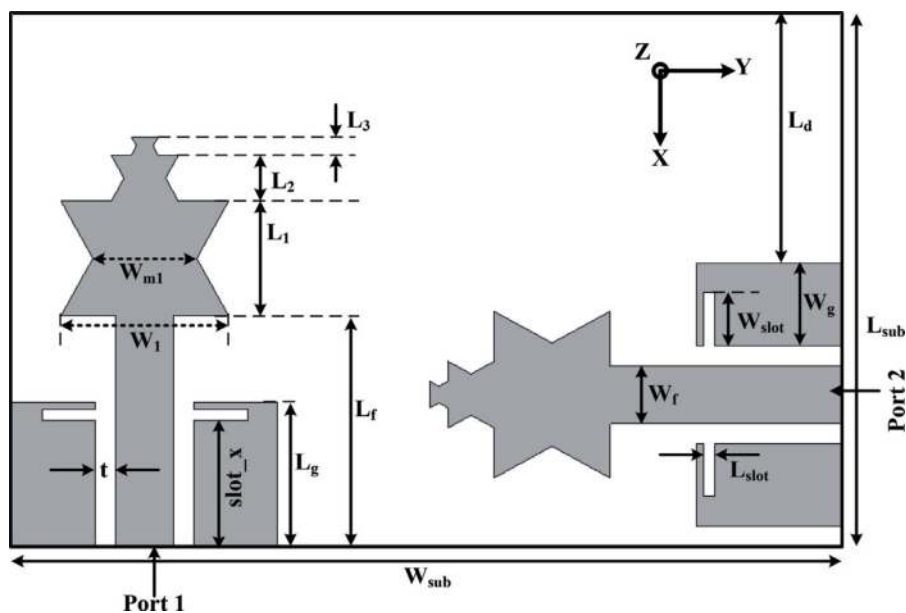
Figure 1.
Geometry of the antenna.

Dimension	Value (in mm)	Dimension	Value (in mm)
L_{sub}	18.5	W_{sub}	28.7
L_g	5	W_g	2.9
L_f	8	W_f	2
L_1	4	W_1	5.8
L_2	1.6	W_{m1}	3.6
L_3	0.64	L_d	8.65
slot_x	4.35	t	0.7
L_{slot}	0.4	W_{slot}	1.85

Table 1.
*Dimensions of the designed polarization diversity antenna.*
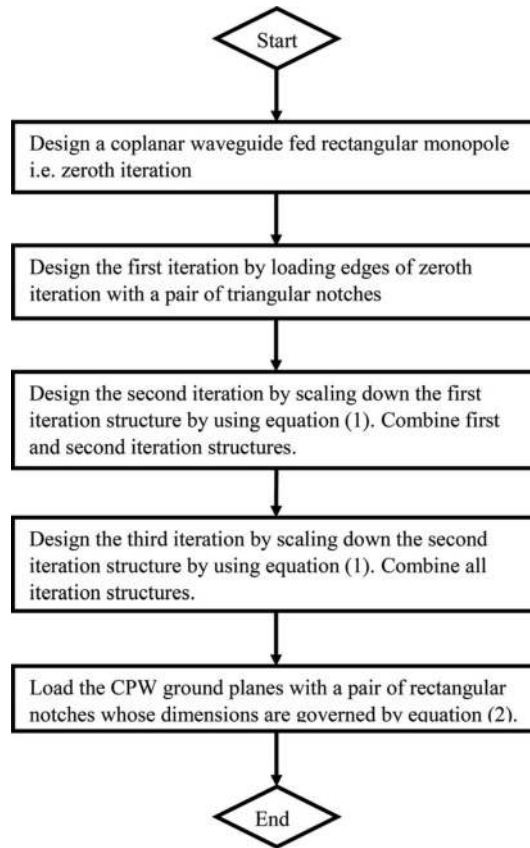
Figure 2.
Flow chart of designing initial radiator geometry.

epoxy substrate having a relative permittivity of 4.4 and loss tangent of 0.02. All the dimensions are optimized by using finite element method (FEM)-based Ansoft's high-frequency structure simulator (HFSS) [30]. During simulation, the radiating patch and ground planes are assumed to be perfect electrical conductors. The antenna structure is designed in two steps.

The fourth iterative fractal geometry of radiator is derived from a rectangular monopole by loading it with a pair of triangular notches on its edges. The flow chart of designing the intermediate design steps is presented in **Figure 2**. The intermediate design steps for radiator geometry are shown in **Figure 3**. The iteration structure dimensions are governed by Eq. (1):

$$R_n = R_{n-1}r^n \qquad (1)$$
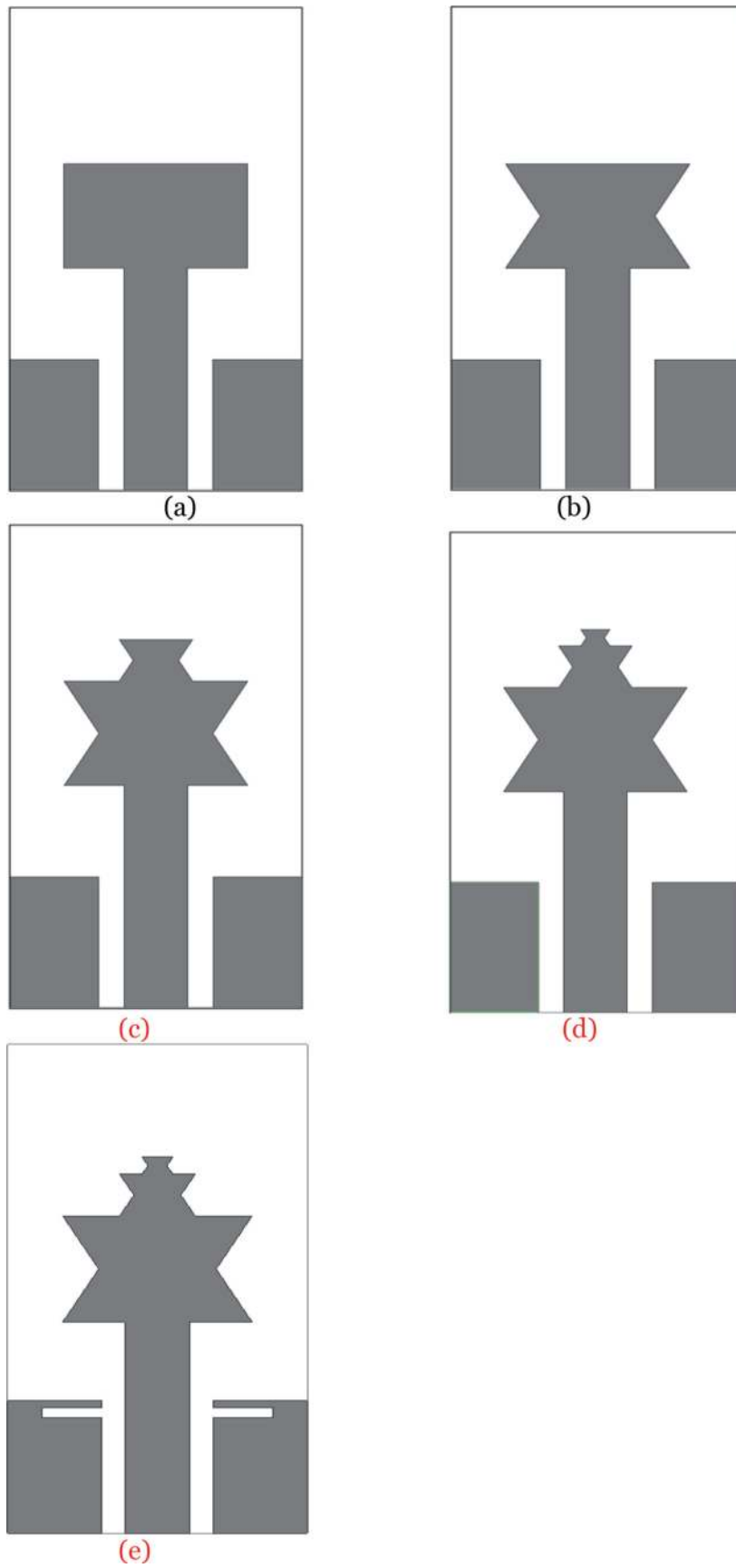
Figure 3.
Designing stages of proposed MIMO antenna element (a) Zeroth iteration, (b) First Iteration (c) Second Iteration (d) Third Iteration (e) Third iteration with ground notch.

where:

n = iteration number = 2 or 3.

R_1 = dimension of the first iteration, i.e. L_1, W_1 and W_{m1}.

R_n = dimension of the nth iteration.

r = iterative ratio = 0.4.

In the first step, the dimensions of radiating patch are unaltered. The bandwidth of inner tapered tree-shaped fractal antenna is enhanced by loading the ground plane with quarter wavelength rectangular notches to excite an additional resonance at 18.6 GHz. The dimensions of notch are governed by Eq. (2):

$$L_r = \frac{c}{4f_r} \approx L_{slot} + 2 \times W_{slot} \qquad (2)$$

L_r = electrical length of slot for resonance.

f_r = resonance frequency = 18.6 GHz.

In the second step, two identical structures designed in the first step are placed orthogonal to each other. The air gap between the two structures and their locations are optimized. All the frequency domain results are calculated by using HFSS. The time domain results and diversity performance parameters are analysed by using CST MWS [31].

3. Results and discussion

The intermediate antenna design steps are compared in terms of their S_{11} curves in **Figure 4**. It is observed that the bandwidth is increasing with an increase in iteration. For further increase in iteration, no significant improvement is observed. The reflection coefficient curves for the initial antenna structure with and without ground notches are illustrated in **Figure 5**. Its quantitative analysis is listed in **Table 2**. It is observed that the lower band edge frequency is negligibly changed, whereas the higher band edge frequency is shifted from 16.4 GHz to 19.4 GHz in the case of notch-loaded ground plane. The initial resonances are slightly shifted to higher frequency with an additional resonance.

3.1 Frequency domain

The designed diversity antenna structure is simulated by using HFSS and CST MWS simulators. The variations of simulated scattering parameters with frequency are demonstrated in **Figure 6**. The quantitative analyses of bandwidth for two antenna elements used in designed antenna structure are presented in **Table 3**. From **Figure 6** and **Table 3**, it is observed that there are some discrepancies among the two simulation results. These discrepancies can be attributed to the different mesh size suitable for numerical techniques on which the simulators are designed. In addition to mesh size, it is also important to mention that in CST MWS the structure can be solved in single pass instead of solution for different frequency spectrum, i.e. 1–2, 2–4, 4–8, 8–16 and 16–32 GHz in HFSS. The differences between the S_{11} and S_{22} characteristics are due to asymmetrical structure with respect to substrate. A good isolation of more than 15 dB is achieved. The designed antenna has resonances at the frequencies of 6, 8, 10.8, 15.8 and 18.8 GHz.

The comparison among the designed antenna and previously reported polarization/pattern diversity antenna structures is listed in **Table 4**. It is observed that the designed antenna has wider bandwidth, good isolation and miniaturized dimensions than other structures.
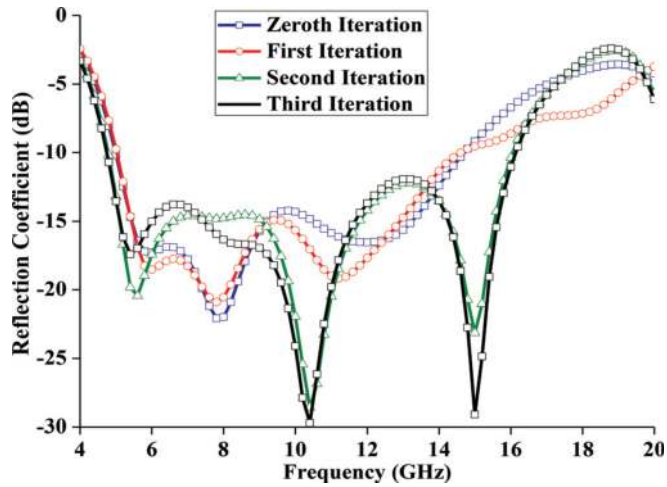
Figure 4.
*Reflection coefficient of intermediate antenna design steps.*
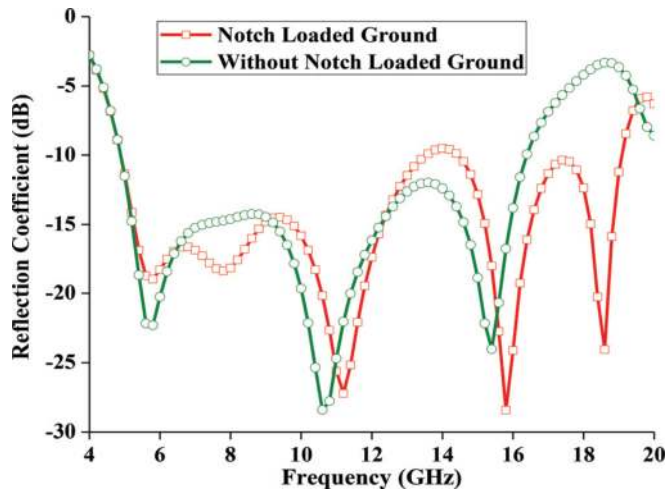
Figure 5.
*Reflection coefficient versus frequency characteristic of single antenna element.*

Antenna	f_L (GHz)	f_H (GHz)	BW (GHz)
Without ground notch	4.9	16.4	11.5
With ground notch	4.8	19.4	14.6

Table 2.
Bandwidth comparison of single antenna element with and without ground notch.

The simulated radiation patterns of two antenna elements at the resonance frequencies of 6, 8, 10.8, 15.8 and 18.8 GHz in all three planes are illustrated in **Figure 7**. From **Figure 7**, it is observed that the antenna structures have bidirectional and omnidirectional patterns at lower frequencies. At higher frequencies, the patterns are distorted omnidirectional in nature due to the excitation of higher-order modes at those frequencies. It is also clearly observable that the patterns of both antenna structures have a phase difference of 90° in each plane as desirable.
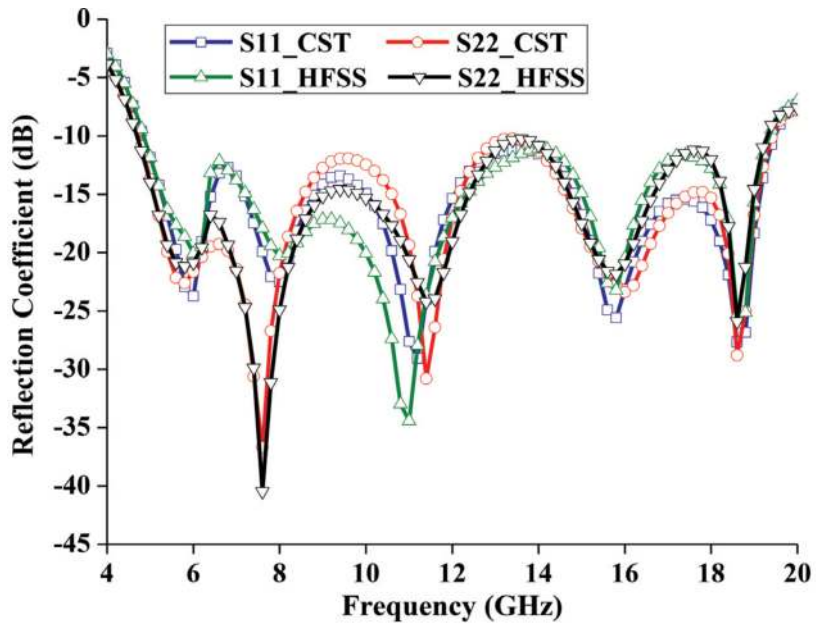
(a)
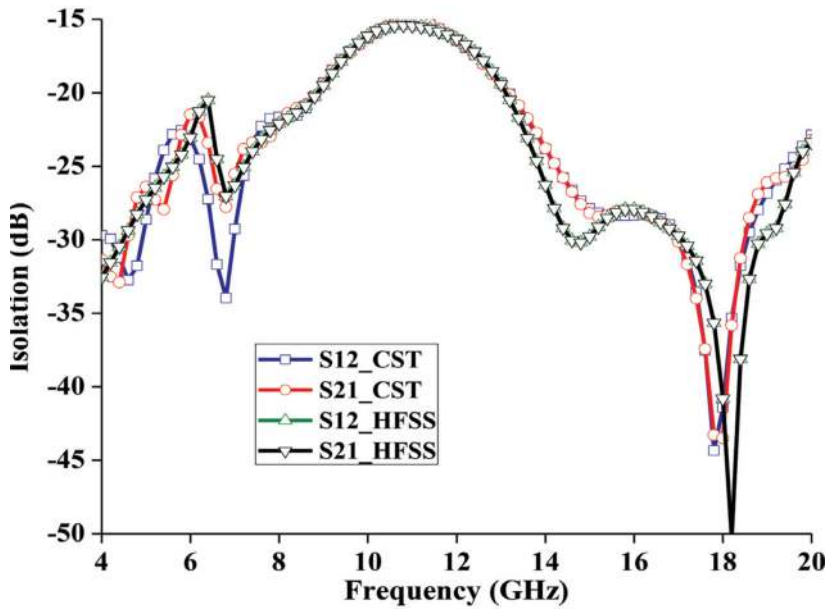
(b)

Figure 6.
Scattering parameters versus frequency characteristics of the designed antenna.

Figure 8 illustrates that the peak realized gain of Antenna I is varying from 0.52 to 4.98 dB with an average of 3.5 dB over the operating frequency band. It also presents that the gain of Antenna II is varying between 1.43 and 3.5 dB with an average of 2.45 dB.

The variations of radiation and total efficiencies with frequency for both antenna elements are shown in **Figure 9**. The radiation efficiencies of both antenna elements are more than 0.7 with an average of more than 0.86. Similarly, the total efficiencies have an average of 0.83. The efficiencies are decreasing with an increase in frequency due to the use of lossy FR-4 substrate.

	Method	f_L (GHz)	f_H(GHz)	BW(GHz)	%BW
Port 1	HFSS	4.85	19.4	14.55	120
	CST MWS	4.84	19.48	14.64	120.4
Port 2	HFSS	4.7	19.3	14.6	121.67
	CST MWS	4.7	19.4	14.7	121.99

Table 3.
Bandwidth of two ports.

S. No.	Chapter	Dimensions (mm²)	Bandwidth (GHz)	Isolation (dB)	% BW	% size reduction
1.	[11]	80×80 mm²	3-12	>15	120	91.7
2.	[14]	34×49 mm²	3.1-10.6	>20	109	68.13
3.	[15]	58×58 mm²	2.8−11	>14	75	84.22
4.	[16]	27×52 mm²	3.25−12	>20	73	62.18
5.	[17]	45×50 mm²	2.7-10.9	>25	121	76.4
6.	[18]	50×50 mm²	2.76-10.75	>15	118	78.76
7.	[19]	23×39.8 mm²	2.5−12	>21	79	42
8.	[20]	80×80 mm²	3-12	>15	120	91.7
9.	[21]	42×81 mm²	3.2-11.2	>20	111	84.39
10.	[22]	21×35 mm²	2.9-11	>20	117	27.76
11.	[23]	24×26 mm²	3.06-11	>18	113	14.91
12.	[24]	28×50 mm²	2.8-11.5	>18	122	62.08
13.	[25]	30×50 mm²	2.5-14.5	>20	141	64.6
14.	[26]	50×85 mm²	2-9.5	>20	130	87.51
15.	[27]	42×30 mm²	3.1-10.6	>20	109	57.86
16.	[28]	16×37.6 mm²	3-12	>19	120	11.74
17.	**Proposed Antenna**	**18.5×28.7 mm²**	**4.7-19.4**	**>15**	**122**	-

Table 4.
Comparison of designed antenna with other UWB diversity antenna.

3.2 Time domain

During time domain analysis, two identical antenna structures are arranged in two major configurations, i.e. face to face and side by side as shown in **Figure 10**. In each of these configurations, one port is excited, whereas the other port is terminated with a matched load. The antenna structure is excited with a Gaussian pulse having a centre frequency of 13 GHz and bandwidth of 1–25 GHz. The normalized amplitudes of the transmitted and received signals are presented in **Figure 11**. From these normalized amplitudes, the correlation between the two signals, i.e. system fidelity factor, is calculated by using Eq. (3). The calculated values of system fidelity factor for four cases are listed in **Table 5**. The values listed in **Table 5** indicate that the signal is slightly distorted in side-by-side configuration in comparison to face-to-face configuration for both cases.

$$F = max \left[\frac{\int_{-\infty}^{\infty} s_t(t)s_r(t+\tau)d\tau}{\int_{-\infty}^{\infty} |s_t(t)|^2 dt \int_{-\infty}^{\infty} |s_r(t)|^2 dt} \right] \quad (3)$$

where $s_t(t)$ and $s_r(t)$ are the transmitted and received pulses and τ is the group delay. The variations of group delay with respect to frequency for all four cases are illustrated in **Figure 12**. It is observed that the group delay has its variations less than 1 ns over the entire band of operation.

3.3 Diversity performance

To analyse the diversity performance of the designed antenna, various parameters like envelope correlation coefficient, diversity gain (DG) and mean effective gain (MEG) are to be calculated from s-parameters or farfield patterns. The envelope correlation coefficient (ECC) signifies the correlation between the radiation patterns of two antenna elements. For the designed antenna structure, ECC (ρ_e) is
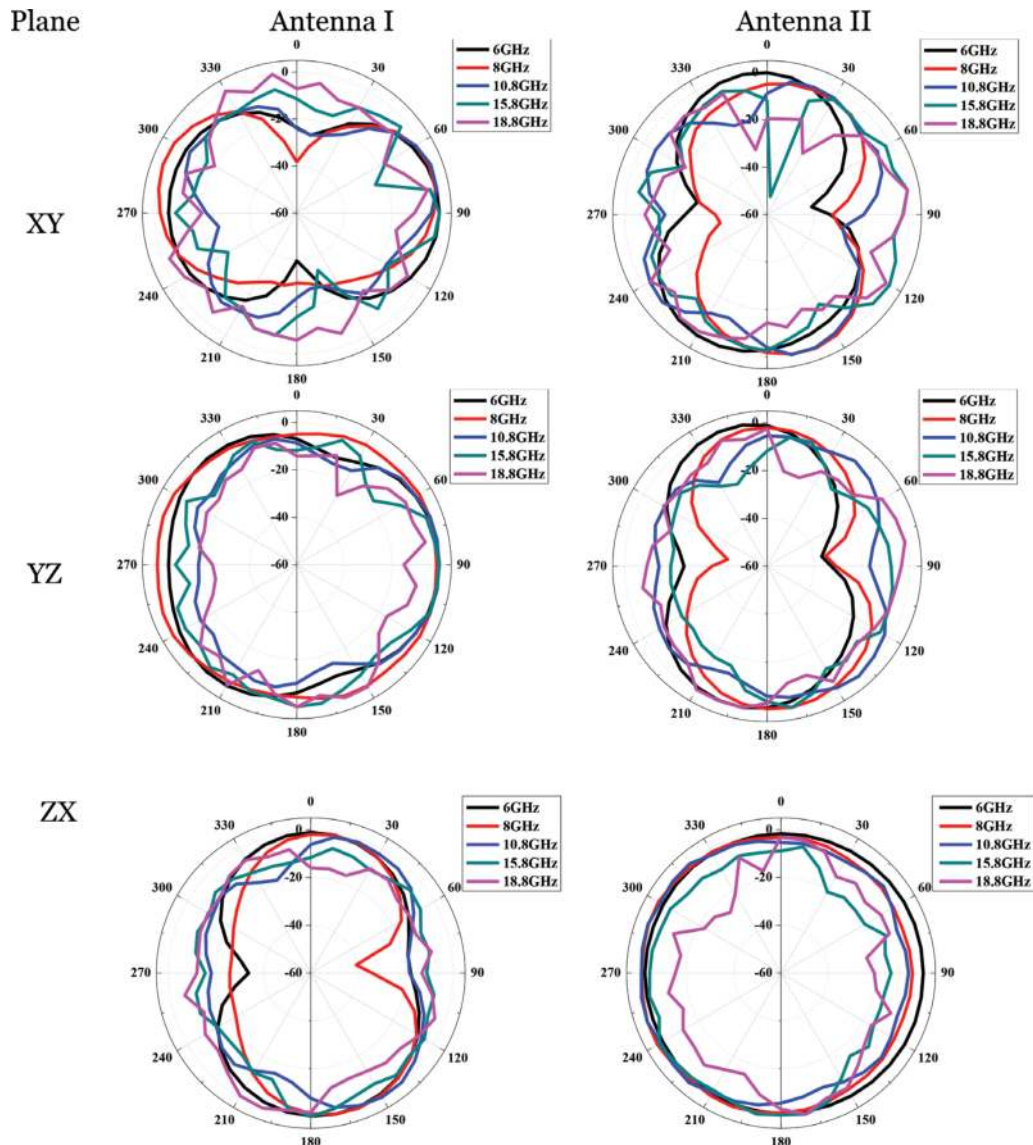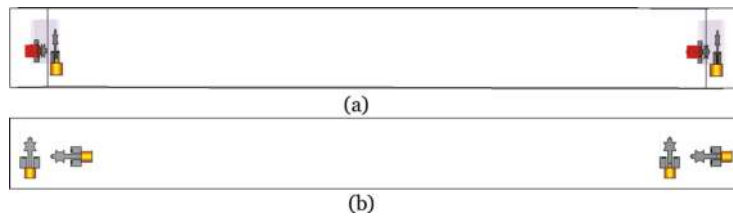

Figure 7.
Radiation patterns of the two antenna elements in XY, YZ and ZX planes.
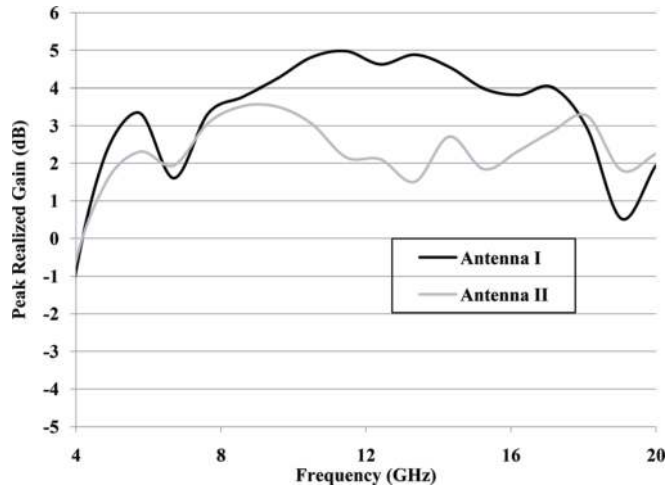
Figure 8.
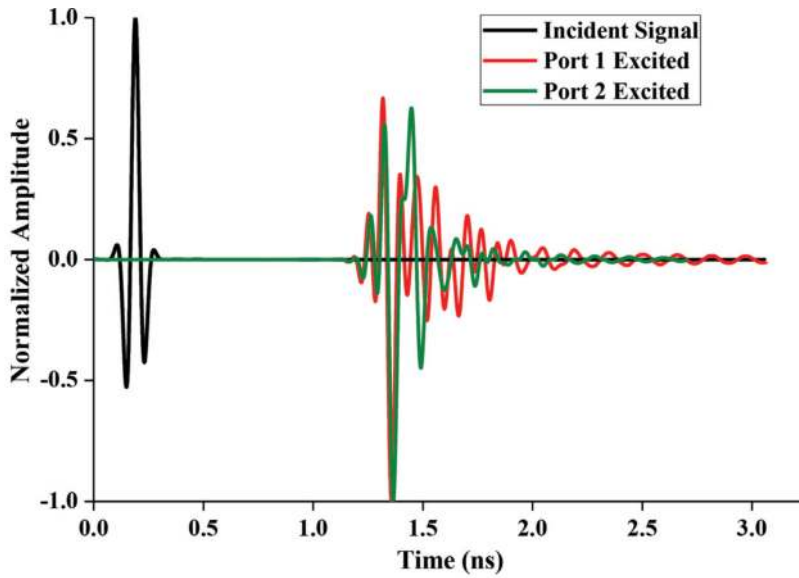*Peak realized gain versus frequency characteristics.*
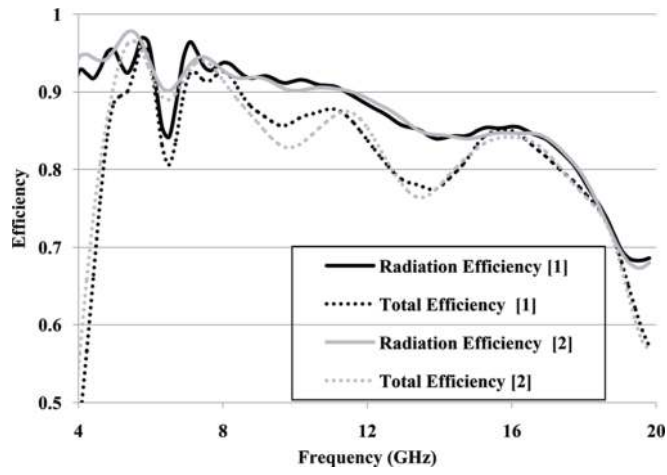
Figure 9.
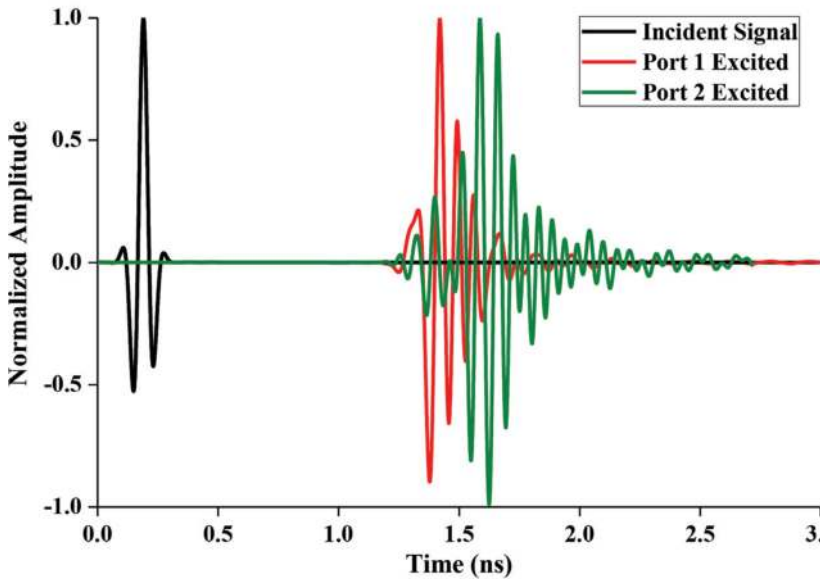*Radiation and total efficiencies of the two antenna elements.*

Figure 10.
Time domain analysis configurations of the diversity antenna. (a) Face to face (b) Side by side.

calculated by using Eq. (4) [32]. The calculated values of ECC are plotted in **Figure 13**.

$$\rho_e = \frac{\left| S_{11}^* S_{12} + S_{21}^* S_{22} \right|^2}{\left(1 - \left(|S_{11}|^2 + |S_{21}|^2 \right) \right) \left(1 - \left(|S_{22}|^2 + |S_{12}|^2 \right) \right)} \tag{4}$$
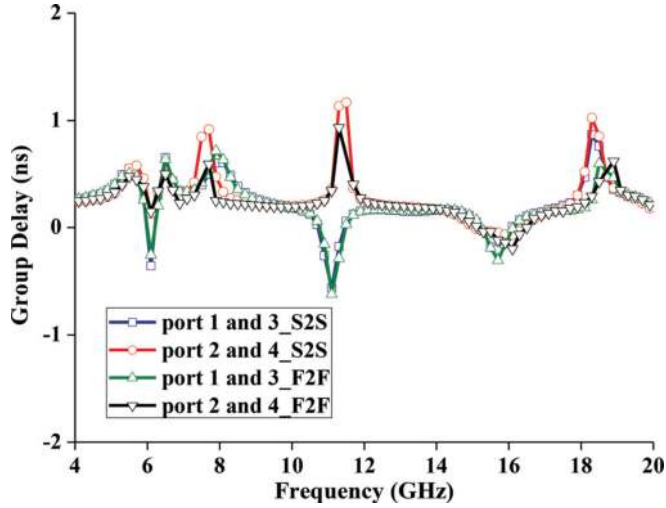
Figure 11.
Normalized amplitudes of the transmitted and received pulses in all four configurations. (a) Face to face (b) Side by side.

System Fidelity Factor	F2F	S2S
Port 2excited	0.79	0.67
Port 1excited	0.88	0.83

Table 5.
System fidelity factor for four configurations of the designed antenna.

From **Figure 13**, it is observed that the ECC values are less than 0.005 in the entire band of operation. These low values of ECC (<0.5) signify that the designed antenna is a good candidate for the UWB applications with polarization diversity [16].

Figure 12.
Group delay versus frequency characteristics of the diversity antenna for all four configurations.
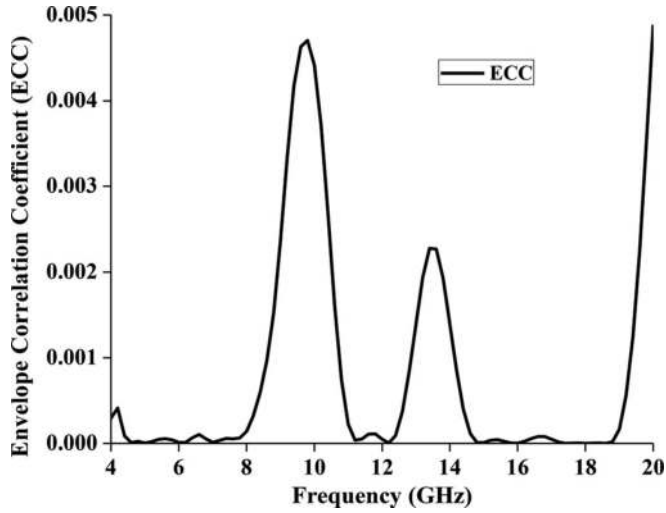
Figure 13.
Envelope correlation coefficient versus frequency characteristic.

The mean effective gain measures the antenna gain of each antenna element taking the radiation power pattern effects, the antenna total efficiency and the propagation effects into account. It is calculated by using Eq. (5) and is plotted for each antenna in **Figure 14**.

$$MEG = \int_{0}^{2\pi} \int_{0}^{\pi} \left[\frac{XPR}{1+XPR} G_\theta(\theta,\varphi)P_\theta(\theta,\varphi) + \frac{XPR}{1+XPR} G_\varphi(\theta,\varphi)P_\varphi(\theta,\varphi) \right] \sin\theta d\theta d\varphi$$

(5)

where XPR represents the cross-polarization ratio, G_θ and G_φ are the θ- and φ-components of the antenna power gain patterns and P_θ and P_φ are the θ- and φ-components of the angular density functions of the incident power, respectively. The MEG values for each antenna element in the case of isotropic radiation, i.e. XPR = 0 dB, are presented in **Figure 14**.

Another important parameter used to identify the suitability of an antenna for diversity applications is diversity gain. It is the difference between the selection combined cumulative distribution function (CDF) and one of the other CDFs at a certain CDF level. The commonly used CDF level is 1% [33]. The DG of the diversity antenna can be calculated approximately by Eq. (6) [34]. From **Figure 15**, it is observed that the diversity gain value is almost constant in the entire band of operation.

$$DG = 10\sqrt{1 - \rho_e} \qquad (6)$$

In the case of a rich multipath environment, the maximum rate of transmission for reliable transmission in a communication channel is estimated by calculating capacity loss (b/s/Hz). For a MIMO antenna, a channel capacity loss of less than 0.4 b/s/Hz is acceptable [35]. It is calculated by using the correlation matrix (7) [35].
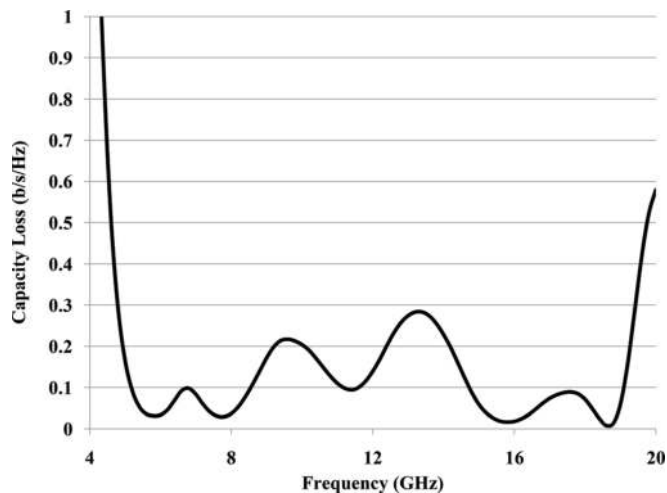
$$C_{loss} = -\log_2\left(\psi^R\right) \qquad (7)$$
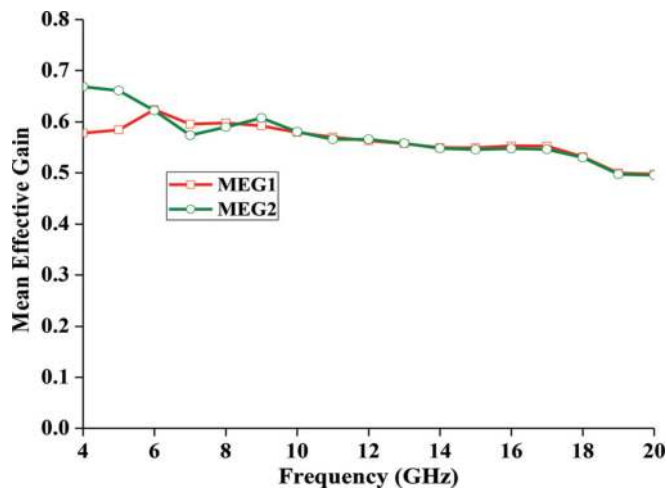
Figure 14.
Mean effective gain versus frequency characteristics of the designed antenna.
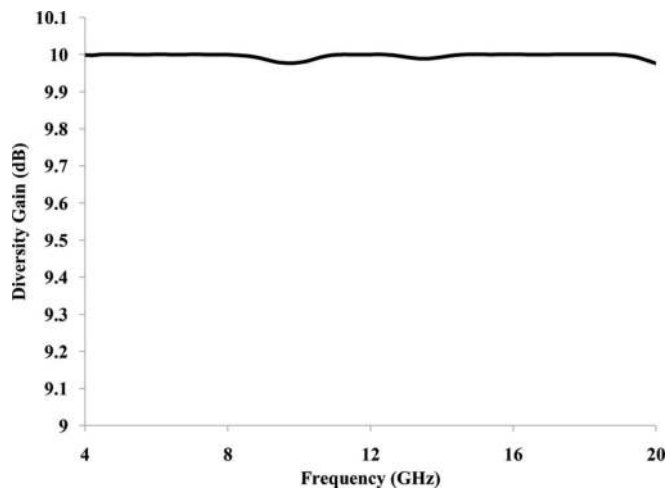
Figure 15.
Diversity gain versus frequency characteristic.

Figure 16.
Capacity loss versus frequency characteristic.

where ψ^R is the correlation matrix of the receiving antenna and is expressed mathematically as

$$\psi^R = \begin{bmatrix} \rho_{11} & \rho_{12} \\ \rho_{21} & \rho_{22} \end{bmatrix} \tag{8}$$

$$\rho_{ii} = 1 - \left(|S_{ii}|^2 + |S_{ij}|^2 \right) \tag{9}$$

$$\rho_{ij} = - \left(S_{ii}^* S_{ij} + S_{ji}^* S_{ij} \right) \tag{10}$$

i, j = 1 or 2.

Figure 16 shows that the channel capacity loss changes with the variation of frequencies. It can be seen that the capacity loss values are always less than 0.3 b/s/Hz in the UWB operating range.

4. Conclusion

A compact third iteration fractal antenna with notch-loaded ground plane for UWB applications is investigated and analysed. By using orthogonal arrangement of two antenna elements, polarization diversity performance is achieved. The designed antenna has an impedance bandwidth of 4.7–19.4 GHz, isolation of more than 15 dB, a size miniaturization up to 92% over previously reported structures and good diversity performance parameters values like ECC < 0.005, almost constant DG = 10 and channel capacity loss of less than 0.3 b/s/Hz which makes it suitable for UWB polarization applications in future wireless communication systems to mitigate the multipath fading.

Author details

Sarthak Singhal[1*] and Amit Kumar Singh[2]

1 Department of Electronics and Communication Engineering, Malaviya National Institute of Technology, Jaipur, Rajasthan, India

2 Department of Electronics Engineering, Indian Institute of Technology (BHU), Varanasi, Uttar Pradesh, India

*Address all correspondence to: sarthak.ece@mnit.ac.in

IntechOpen

References

[1] Federal Communication Commission. "First order and report: Revision of part 15 of the Commission's rules regarding UWB transmission systems," April 22, 2002

[2] Dietrich CB Jr, Dietze K, Nealy JR, Stutzman WL. Spatial, polarization, and pattern diversity for wireless handheld terminals. IEEE Transactions on Antennas and Propagation. 2001;**49**(9):1271-1281

[3] Allen B, Dohler M, Okon E, Malik WQ, Brown AK, Edwards D. UWB Antenna and Propagation for Communications, Radar and Imaging. Hoboken, NJ, USA: Wiley; 2007

[4] Wang A, Zhenghe F, Luk K-M. Pattern and polarization diversity antenna with high isolation for portable wireless devices. IEEE Antennas and Wireless Propagation Letters. 2009;**8**: 209-211

[5] Naraghi-Pour M, Ikuma T. "Diversity techniques for spectrum sensing in fading environments," presented at the MILCOM; 2008

[6] Gkonis P, Tsoulos G, Kaklamani D. Dual code Tx diversity with antenna selection for spatial multiplexing in MIMO-WCDMA networks. IEEE Communications Letters. 2009;**13**(8): 570-572

[7] Boyle K. Radiation patterns and correlation of closely spaced linear antennas. IEEE Transactions on Antennas and Propagation. 2002;**50**(8): 1162-1165

[8] Wei K, Zhang Z, Chen W, Feng Z. A novel hybrid-fed patch antenna with pattern diversity. IEEE Antennas and Wireless Propagation Letters. 2010;**9**: 562-565

[9] Yang SLS, Luk K-M, Lai H-W, Kishk A-A, Lee K-F. A dual-polarized antenna with pattern diversity. IEEE Antennas and Propagation Magazine. Dec. 2008; **50**(6):71-79

[10] Huang Y, Nehorai A, Friedman G. Mutual coupling of two collocated orthogonally oriented circular thin-wire loops. IEEE Transactions on Antennas and Propagation. 2003;**51**(6): 1307-1314

[11] Gallo M, Daviu EA, Bataller MF, Bozzetti M, Pardo JMMG, Llacer LJ. A broadband pattern diversity annular slot antenna. IEEE Transactions on Antennas and Propagation. 2012;**60**(3): 1596-1600

[12] Bao XL, Ammann MJ. Wideband dual-frequency dual-polarized dipole-like antenna. IEEE Antennas and Wireless Propagation Letters. 2011;**10**: 831-834

[13] Adamiuk G, Zwick T, Wiesbeck W. Compact, dual-polarized UWB-antenna, embedded in a dielectric. IEEE Transactions on Antennas and Propagation. 2010;**58**(2):279-286

[14] Yoon HK, Yoon YJ, Kim H, Lee CH. Flexible ultra-wideband polarisation diversity antenna with band-notch function. IET Microwaves, Antennas and Propagation. 2011;**5**(12):1463-1470

[15] Chacko BP, Augustin G, Denidni TA. Uniplanar slot antenna for ultrawideband polarization diversity applications. IEEE Antennas and Wireless Propagation Letters. 2013;**12**: 88-91

[16] Koohestani M, Moreira AA, Skrivervik AK. A novel compact CPW-fed polarization diversity ultrawideband antenna. IEEE Antennas and Wireless Propagation Letters. 2014; **13**:563-566

[17] Femina BS, Mishra SK. Compact WLAN band-notched printed ultrawideband MIMO antenna with polarization diversity. Progress in Electromagnetics Research. 2016;**61**: 149-159

[18] Chacko BP, Augustin G, Denidni TA. Uniplanar polarisation diversity antenna for ultrawideband systems. IET Microwaves, Antennas and Propagation. 2013;**7**(10):851-857

[19] Khan MS, Capobianco AD, Naqvi A, Ijaz B, Asif S, Braaten BD. Planar, compact ultra-wideband polarisation diversity antenna array. IET Microwaves, Antennas and Propagation. 2015;**9**(15):1761-1768

[20] Daviu EA, Gallo M, Clemente BB, Bataller MF. Ultrawideband slot ring antenna for diversity application. Electronics Letters. 2010;**46**(7):478-480

[21] Srivastava K, Kumar A, Kanaujia BK, Dwari S, Kumar S. A CPW-fed UWB MIMO antenna with integrated GSM band and dual band notches. International Journal of RF and Microwave Computer-Aided Engineering. 2018;**29**(1):1-10

[22] Biswal SP, Das S. A compact dual port UWB-MIMO/diversity antenna for indoor application. International Journal of Microwave and Wireless Technologies. 2017;**10**(03):360-367

[23] Biswal SP, Das S. A compact printed ultra-wideband multiple-input multiple-output prototype with band-notch ability for WiMAX, LTEband43, and WLAN systems. International Journal of RF and Microwave Computer-Aided Engineering. 2019;**6**:1-11

[24] Ibrahim AA, Machac J, Shubair RM. Compact UWB MIMO antenna with pattern diversity and band rejection characteristics. Microwave and Optical Technology Letters. 2017;**59**(6): 1460-1464

[25] Iqbal A, Saraereh OA, Ahmad AW, Bashir S. Mutual coupling reduction using F-shaped stubs in UWB-MIMO antenna. IEEE Access. 2018;**6**:2755-2759

[26] Zhao X, Yeo SP, Ong LC. Planar UWB MIMO antenna with pattern diversity and isolation improvement for Mobile platform based on the theory of characteristic modes. IEEE Transactions on Antennas and Propagation. 2018; **66**(1):420-425

[27] Yadav D, Abegaonkar MP, Koul SK, Tiwari VN, Bhatnagar D. Two element band-notched Uwb Mimo antenna with high and uniform isolation. Progress in Electromagnetics Research. 2018;**63**: 119-129

[28] Sipal D, Abegaonkar MP, Koul SK. Compact dual band-notched UWB MIMO antenna for USB dongle application with pattern diversity characteristics. Progress in Electromagnetics Research. 2018;**87**: 87-96

[29] Singhal S, Goel T, Singh AK. Inner tapered tree shaped fractal antenna for UWB applications. Microwave and Optical Technology Letters. 2015;**57**(3): 559-567

[30] HFSS, "High Frequency Structure Simulator ver. 11, Finite Element Package."Ansoft Corporation. 2009. Available from: http://www.ansoft.com

[31] CST Microwave Studio Suite 2011. CST Inc.; 2007

[32] Blanch S, Romeu J, Corbella I. Exact representation of antenna system diversity performance from input parameter description. Electronics Letters. 2003;**39**(9):705-707

[33] Kildal PS, Rosengran K. Correlation and capacity of MIMO systems and coupling, radiation efficiency, diversity gain of their antennas: Simulations and measurements in a reverberation

chamber. IEEE Communications
Magazine. 2004;**42**(12):102-112

[34] Gao Y, Chen XD, Ying ZN. Design
and performance investigation of a
dual-element PIFA array at 2.5 GHz for
MIMO terminal. IEEE Transactions on
Antennas and Propagation. 2007;**55**(12):
3433-3441

[35] Tripathi S, Mohan A, Yadav S. A
compact Koch fractal UWB MIMO
antenna with WLAN band-rejection.
IEEE Antennas and Wireless
Propagation Letters. 2015;**14**:1565-1568